COBEM 2021 26th International Congress of Mechanical Engineering
November 22-26, 2021, Virtual Congress, Brazil

COB-2021-0317
ANALYTICAL AND NUMERICAL STUDY OF THE CONTACT STRESS FIELD BETWEEN TWO CURVED SURFACES WITH AN ELLIPTICAL SHAPE IN A CROWNED GEAR

Geraldo Cesar Rosario de Oliveira
Fernando de Azevedo Silva
UNESP - Faculdade de Engenharia de Guaratinguetá, Avenida Ariberto Pereira da Cunha 333, Guaratinguetá, 12500-000, Brasil.
e-mail: geraldo.cesar@unesp.br
e-mail: fernando.azevedo@unesp.br

Abstract. *In this article, contact stress field between two gears was approximated as ellipsoidal curved surfaces according to generalized contact theory. Crowned teeth have surfaces modified lengthwise to produce localized contact. A static load was used to compare the results obtained in the numerical and analytical methods using general equation proposed by Hertz. Numerical methods applied in ANSYS® were Pure Penalty, Normal Lagrange and Multi-Point Constraint. Considering normal contact stress, Pure Penalty method in convex-convex configuration obtained result closest to analytical method while Normal Lagrange method obtained least difference in case convex-concave. It was proven that shear stress as expected, has a lot of influence on result, mainly on equivalent stress and normal Lagrange method obtained results closer to analytical method in this regard.*

Keywords: *Contact stress field, Finite elements, Hertz stress, Gear teeth modifications.*

1. INTRODUCTION

Crowning or barreling is the bulging of the tooth face from the center to the reaching edge and is usually described as a circular arc profile, making the tooth surface slightly convex. This method allows the gear to maintain contact in central region of tooth and avoids the contact of edge. Use of crowning (Kubota and Nyumon, 2010; Bergseth and Björklund, 2010) shifts peak load from tooth flank edges and therefore reduces the risk for high contact pressures at edges.

Gear teeth modifications such as lead crowning are often recommended to compensate for misalignment. Defect can occur even if gears themselves are correct. Assembly process may present errors of parallelism of two axes or eccentricity when assembling gears in axes. This is due to other elements that generate interference caused by inaccurate machining of the casting, housing, shafting, gearboxes, or bearing journals (KHK, 2021). It is also important to consider contact stresses between gears because of contact fatigue. Contact fatigue differs from the classic structural fatigue generated by flexion or torsion because it results from a state of contact or hertzian tension. This state of localized tension occurs when the curved surfaces are in contact under a normal load (Brezeanu, 2015; Azarov and Zhuravlev, 2017; Purushothaman and Thankachan, 2014) and when one surface moves over the other as in a pair of gears (Hwang et al, 2013) or in contact of a roller on a track in a bearing (Guidi and Silva, 2013). In this fatigue mode, the failures are initiated by alternating subsurface shear stresses associated with compression stresses at the contact (Chandra et al, 2016). Removal of material or fragmentation occurs due to the propagation of micro-cracks generated by the underground plastic deformation that accumulates with increasing cycles (Tallian, 1967; Rycerz et al, 2017).

The objective of the study in this paper is to better understand the numerical methods cited in other studies on contact compared to the analytical method using the general contact equation of Hertz as an approximation in case the gear tooth faces have concave and convex profiles for understand the contact mechanism in this state.

2. ANALYTICAL ANALYSIS OF CONTACT

The contact interactions were studied in two cases. First case was between two identical crowned spur gears acting as convex-convex configuration model. In second convex-concave case, contact occurred (hypothetically for the study) between a crowning gear and a non-standard spur gear inspired by Andrei (2005) work whose face width is curved with modified geometry. The crowned gear studied was generated from modification of a spur gear of module equal to 3 with 20 teeth. The face and flank were modified by shifting the lateral and upper corners, generating a crowning thickness of 0.2 mm, keeping the envolvental curve in center of face and flank. The two solids generated are illustrated in Figure 1. The altered gears, in both situations, maintain contact only in the central region of the tooth (pitch circle) and avoid the contact of the edge.

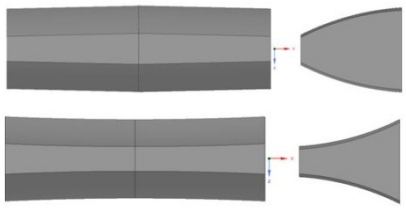

Figure 1. The models of solids generated: the first with a concave surface and the second with a convex surface.

In general case when solids are pressed by an external force, they create a contact area delimited by an ellipse as shown in Figure 2. In the contact region, tractions occur in the normal and tangential directions due to external loading. These tangential and normal tensions are accompanied by an elastic field of displacements, deformations and stresses in the bodies (Kalker, 1990). From this, using this theoretical foundation known as generalized contact case, the aim of article was to understand the behavior of the elastic field of stresses on the surface of bodies where the contact phenomena occur. The study follows the generalized case according to the Hertz assumptions (Purushothaman and Thankachan, 2014; Juvinall and Marshek, 2008; Timoshenko and Goodier, 1970): Contact surface is slightly curved; Stress-strain state is subjected to the linear elasticity theory; Contact surfaces are frictionless; Bodies in contact are elastic, isotropic, homogeneous and smooth.

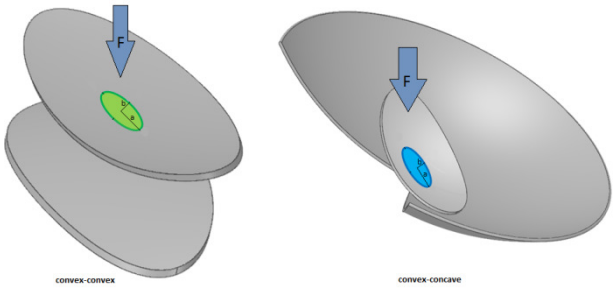

Figure 2. Contact region between solids.

According to Eq. (1) (Juvinall and Marshek, 2008; Timoshenko and Goodier, 1970; Sackfield and Hills, 1983) defines the force ***F*** acting between two solid is equal to volume of semi-ellipsoid generated by semi-diameters ***a*** and ***b*** of the elliptical region. Maximum pressure p_{max} due to this interaction occurs at the center of the elliptical contact surface.

$$F = \iint p dA = \left(\frac{2}{3}\pi ab\right) p_{max} \tag{1}$$

The semi-diameters ***a*** and ***b*** are defined from Eq. 2 and Eq. 3 (Norton, 2013; Juvinall and Marshek, 2008):

$$a = k_a \sqrt[3]{\frac{3F\left(\frac{1-\nu_1^2}{E_1}+\frac{1-\nu_2^2}{E_2}\right)}{4A}} \tag{2}$$

$$b = k_b \sqrt[3]{\frac{3F\left(\frac{1-\nu_1^2}{E_1}+\frac{1-\nu_2^2}{E_2}\right)}{4A}} \tag{3}$$

Where:
F is the force acting on the system;
ν_1 and ν_2 are the Poisson's ratio of solids 1 and 2;
E_1 and E_2 are the elasticity modules of solids 1 and 2;
k_a and k_b are coefficients dependent on geometric constants of solids 1 and 2 according to equations 4 and 5 (Norton, 2013; Juvinall and Marshek, 2008);

$$k_a = 50.192\phi^{-0,86215} \tag{4}$$

$$k_b = 0.0045333 + 0.043581\phi - 0.0017292\phi^2 + 3.7374E-5\phi^3 - 3.7418E-7\phi^4 + 1.4207E-9\phi^5 \quad (5)$$

$\phi$is defined by $cos^{-1}\left(\frac{B}{A}\right)$. Geometric constants $\boldsymbol{A}$ and $\boldsymbol{B}$ depend on radius of curvature of solids in contact according to Eq. 6 and Eq. 7 (Norton, 2013; Juvinall and Marshek, 2008):

$$A = \frac{1}{2}\left(\frac{1}{R_1} + \frac{1}{R_1'} + \frac{1}{R_2} + \frac{1}{R_2'}\right) \quad (6)$$

$$B = \frac{1}{2}\left[\left(\frac{1}{R_1} - \frac{1}{R_1'}\right)^2 + \left(\frac{1}{R_2} - \frac{1}{R_2'}\right)^2 + 2\left(\frac{1}{R_1} - \frac{1}{R_1'}\right)\left(\frac{1}{R_2} - \frac{1}{R_2'}\right)cos2\theta\right]^{\frac{1}{2}} \quad (7)$$

$R_1, R_1'$are the radius of solid 1;
$R_2, R_2'$are the radius of solid 2;

Properties of gears are in Table 1.

Table 1. Gear properties.

Properties	Convex profile gear	Concave profile gear
Poisson's ratio	0.29	0.29
Elasticity module, GPa	207	207
External force, N	100	100
R, mm	18	-25
R', mm	189	-250

The angle $\boldsymbol{\theta}$ (in degrees) occurs between planes containing the radius R_1 and R_2 of two bodies. In case of cavities the radius will be negative.

Equations 8, 9 and 10 refer to main stresses acting on center line on surface of bodies (Juvinall and Marshek, 2008; Timoshenko and Goodier, 1970; Sackfield and Hills, 1983). These stresses are compressive and their values are maximum on the surface. The tensions decrease significantly, increasing the depth and the distance from the center line.

$$\sigma_x = -\left[2\nu + (1-2\nu)\frac{b}{a+b}\right]p_{max} \quad (8)$$

$$\sigma_y = -\left[2\nu + (1-2\nu)\frac{a}{a+b}\right]p_{max} \quad (9)$$

$$\sigma_z = -p_{max} \quad (10)$$

Maximum shear stress below surface due to normal stresses in xy plane is defined according to Eq. (11) (Juvinall and Marshek, 2008; Timoshenko and Goodier, 1970).

$$\tau_{xy} = 0{,}304p_{max} \quad (11)$$

Equivalent stress σ' Eq. (12) is hypothetical uniaxial tensile stress that would produce same distortion energy that is created by the actual combination of actual stresses involved in solid (Norton, 2013; Juvinall and Marshek, 2008).

$$\sigma' = \sqrt{\sigma_x^2 + \sigma_y^2 - \sigma_x\sigma_y + 3\tau_{xy}^2} \quad (12)$$

3. NUMERIC SIMULATION

The commercial software ANSYS® was used for the development the application of the numerical method in convex-convex and convex-concave contacts in the Static Structural module of the Workbench. The steps of this study are illustrated in flowchart form in Chart 1:

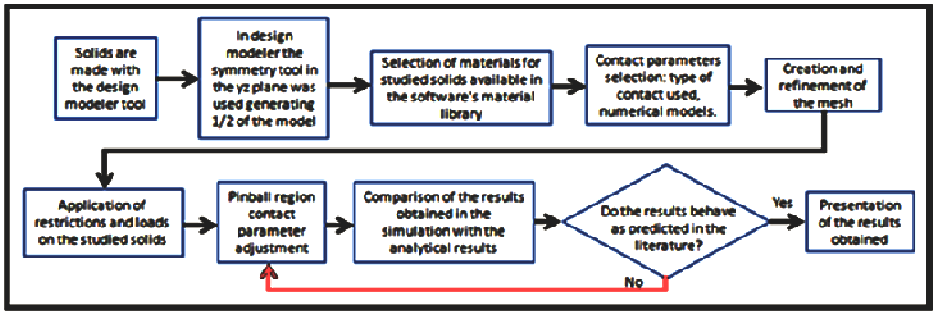

Chart 1. Study stages.

3.1 Development of solids and selection of materials

The solids of the two studied contact configurations are developed in design modeler tool. In this study the altered gears, in both situations, maintain contact only in the central region of tooth (pitch circle) and avoid the contact of the edge. This assumes the simplification of the case for the pair of teeth in contact. The symmetry tool in the yz plane was used generating 1/2 of the model in Design Modeler in both configurations as shown in Figure 3 this feature reduces processing time and allows a greater number of elements in the mesh.

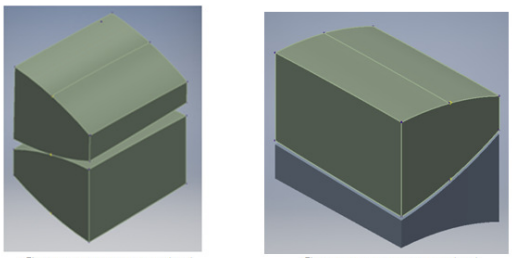

Figure 3. Solids generated in the software.

The material used in the solids was the structural steel available in the software material library with Poisson's ratio of 0.3, elastic modulus of 207 GPa, tensile yield strength equal 250 MPa and tensile ultimate strength equal 460 MPa. This material has the mechanical properties similar to the gears listed in Table 1.

3.2 Definition of contact parameters and numerical methods used

The algorithms used were Pure Penalty, Multi-Point Constraint (MPC) and Normal Lagrange. A summary comparison of the characteristics and particularities of the methods according to (ANSYS, 2015b) are presented in Chart 2:

Pure Penalty	Normal Lagrange	Multi-Point Constraint
Good convergence behavior (few equilibrium iterations).	Additional equilibrium iterations if needed chattering is present.	Good convergence behavior (few equilibrium iterations).
Sensitive to selection of normal contact stiffness.	No normal contact stiffness is required.	No normal contact stiffness is required.
Contact penetration is present and uncontrolled.	Usually, penetration is near-zero.	No Penetration.
Useful for any type of contact behavior.	Useful for any type of contact behavior.	Only Bonded & No Separation behaviors.
Contact detection at integration points.	Contact Detection at Nodes.	Contact Detection at Nodes.

Chart 2. Characteristics and particularities of the methods. Adapted from (ANSYS, 2015b).

The penalty method involves adding a penalty term to enhance the solving process. This method is characterized by the use of a penalty term to improve the solution. In the case of contact problems the penalty term includes the stiffness matrix on the analyzed contact surface. The matrix results from the concept of imaginary penetration resistance between bodies (Stefancu et al 2011; ANSYS, 2007a).

Lagrange Formulation adds an extra degree of freedom as contact pressure to satisfy contact compatibility (Lanoue et al 2009). Consequently, instead of resolving the contact force such as contact stiffness and penetration, the contact force (contact pressure) is explicitly resolved as an extra constraint (Hattori and Serpa, 2015). The Normal Lagrange method is so named because the Lagrange multiplier formula is used in the normal direction, while the penalty-based method is used in the tangential direction (Lanoue et al 2009).

The MPC internally adds constraint equations to trap the displacements between the contact surfaces. This approach is not based on the previous methods. It is a direct and efficient way of relating surfaces of contact regions that are hurried or connected (Zhang et al, 2012; Xie and Feng, 2009).

In options of the contact were used "Contact stiffness factor" equal to 0.1, "pinball region" equal to 10 µm and the contact defined by "No separation" considering that the components always touch during loading (Guidi and Silva, 2013). The "pinball region" is a parameter of contact element that differentiates between the status of the open or closed field. It can be thought of as a spherical boundary around each point for contact detection (Guidi and Silva, 2013).

3.3 Mesh development and application of restrictions and loads

Convex-convex configuration was generated automatically with the element SOLID187 used for irregular 3-D mesh (Guidi and Silva, 2013) with the resources adaptive sizing, transition fast, smoothing medium and mesh refining was used on the contact faces of the cylinders, and the refining on the was done with option 3 in the contact faces. In this case the options refer to the refinements of the mesh made automatically reducing the size of the elements, option 3 means the use of the smallest elements, that is, a denser mesh. It is advantageous to use this feature in this study because of the relatively small size of the models and their simple formats. The use of this tool generates the finest and most homogeneous mesh in a pre-established way without spending a lot of resources and processing time. Refinement of meshes on surfaces in contact makes it possible to generate a reliable model with more accurate results. While a mesh with coarser elements can generate errors or difficulties in the convergence of results, especially when it comes to the study of the contact interface, uncertain results can occur due, for example, to false contact detection or surface penetration.

Restrictions used in this system limit the movement of drive gear tooth in directions of x and y axes while the driven gear tooth is restricted in all axes. The external load used has an intensity of -100 N in the direction of the z axis. All of these procedures are illustrated in Figure 4.

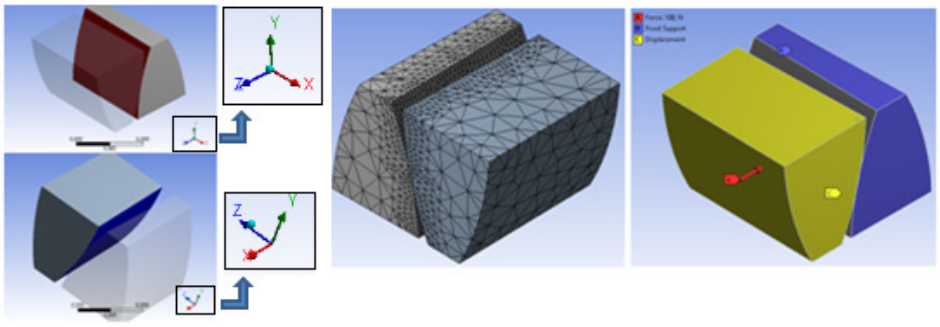

Figure 4**.** Contact regions, mesh profile and restrictions assigned in the convex-convex model.

In other case, convex-concave, mesh was automatically generated with the element SOLID187, the procedures are illustrated in Figure 5. Mesh refining was used on the surfaces that touch during the loading; both were generated with option 3. The concave solid (driven gear tooth) received restrictions on all axes and the convex (drive gear tooth) only moves on the z-axis. The load assigned to drive gear tooth was identical to that used in case of convex-convex of -100 N on the z-axis.

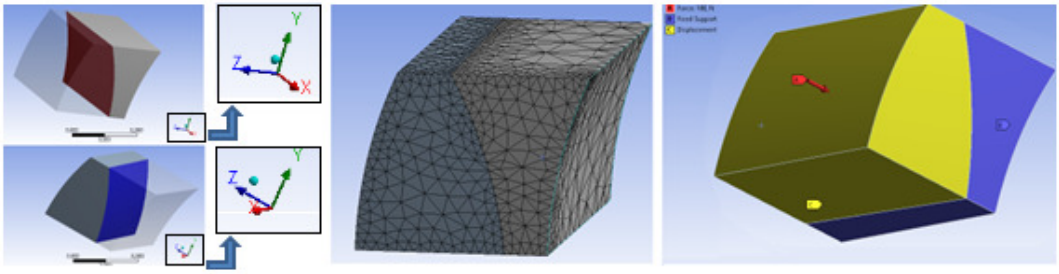

Figure 5. Contact regions, mesh profile and restrictions assigned in the cylindrical convex-concave model.

3.4 Adjusting the pinball region tool and comparing results

The pinball region parameter defines how far the contact surfaces are separated, that is, it differentiates if the contact is "far field open" or "near field open" in each interaction. This element acts within a spherical area defining the limits of each contact detection point. For example, if a node is inside this sphere at the contact interface of the target surface, the software checks this area after each interaction in search of contact detection. However, elements outside this sphere are considered distant and will not be monitored between interactions (ANSYS, 2015b).

In this study, contact was defined as no separation and this influences the behavior of the pinball region. In this case, the software considers as closed contact the elements of the contact and target surfaces within this region. In the case of curved surfaces, the software can consider that the nodes and distant elements are in contact if the pinball radius is greater than necessary, generating excessive restrictions on the contact matrix. From that, a manual interaction method was used, increasing the pinball radius to 100 µm and then 500 µm for the results to converge according to the results of the analytical method.

4. RESULTS

Results obtained from stress values generated in the contact of two configurations studied using the analytical and numerical methods are shown in Table 2 and Table 3. For greater approximation with the analytical method, interactive mode was used for all methods.

Table 2. Results of convex-convex configuration.

Method used in convex-convex contact				
Stress	Analytical	Pure Penalty	Normal Lagrange	MPC
Equivalent	761.670 MPa	763.850 MPa	777.680 MPa	589.250 MPa
Normal	768.800 MPa	751.160 MPa	871.510 MPa	915.960 MPa
Shear	48.780 MPa	50.986 MPa	50.802 MPa	45.970 MPa

Table 3. Results of convex-concave configuration.

Method used in cylindrical body in a cylindrical cavity contact				
Stress	Analytical	Pure Penalty	Normal Lagrange	MPC
Equivalent	207.680 MPa	188.720 MPa	162.510 MPa	821.550 MPa
Normal	201.100 MPa	204.430 MPa	200.230 MPa	948.950 MPa
Shear	12.001 MPa	9.234 MPa	6.017 MPa	23.953 MPa

Percentage differences obtained between results are shown in Table 4 and Table 5.

Table 4. Differences between results in convex-convex contact.

Compared Methods			
Stress	Analytical / Pure Penalty	Analytical / Normal Lagrange	Analytical / MPC
Equivalent	0.286%	2.102%	12.811%
Normal	2.294%	13.360%	19.142%
Shear	4.522%	4.145%	5.761%

Table 5. Differences between results in convex-concave contact.

Compared Methods			
Stress	Analytical / Pure Penalty	Analytical / Normal Lagrange	Analytical / MPC
Equivalent	9.129%	21.750%	295.585%
Normal	1.656%	0.433%	99.608%
Shear	23.050%	49.858%	371.880%

The small differences found in the convex-convex case between the compared methods were between 0.2% and 4% using Pure Penalty. While in the other case convex-concave the minor differences between the methods occur using Normal Lagrange ranging from 0.4% to 49%. The lowest result between the comparisons occurred with the Pure Penalty method in the convex-convex configuration considering only the normal tension with a difference 0.286%.

From results of analytical method was obtained the behavior of contact stresses normalized in reaction to depth, illustrated in Figure 6. Normal compressive stress σ_z, decreases with the depth below the elliptical contact surface as well as the behavior of σ_x and σ_y.

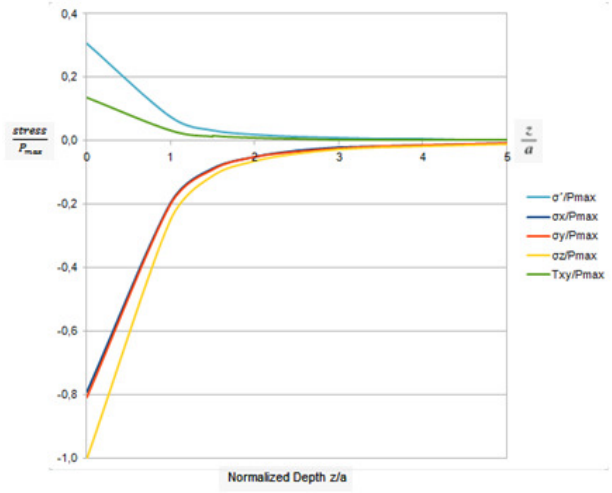

Figure 6. Normalized stresses as a function of depth.

Material is subjected to action of force in negative direction of z-axis and tends to expand in x and y directions due to Poisson's ratio (Köhn and Silva, 2020a; Köhn and Silva, 2020b; Norton, 2013; Juvinall and Marshek, 2008). Therefore, the material cannot move within this region of acting pressure and reacts by generating compressive forces in the x and y directions. Due to symmetrical shape of load, stresses in x, y and z directions, shown graphically in Fig. 6 are the main stresses (Köhn and Silva, 2020a). Shear stress has positive values and according to (Norton, 2013) have maximum value just below surface. In this case, as shown in Figure 6 equivalent stress has a curve behavior similar to that of shear due to its great influence on material distortion (Köhn and Silva, 2020a).

In Figures 7-9 the results of methods used in convex-convex contact configuration were illustrated. Regions present a significant difference in amplitude of gradients resulting in normal and shear stress, while regions delimited by equivalent stress are similar in MPC and Lagrange methods.

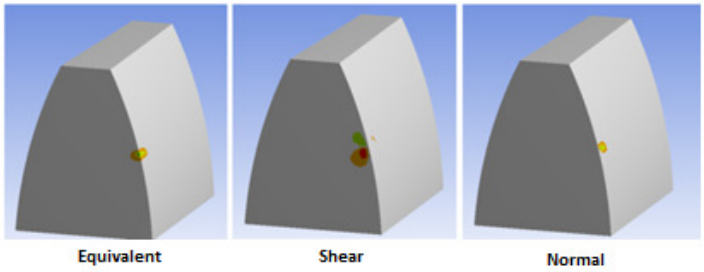

Figure 7. Stresses in convex-convex contact using Pure Penalty method.

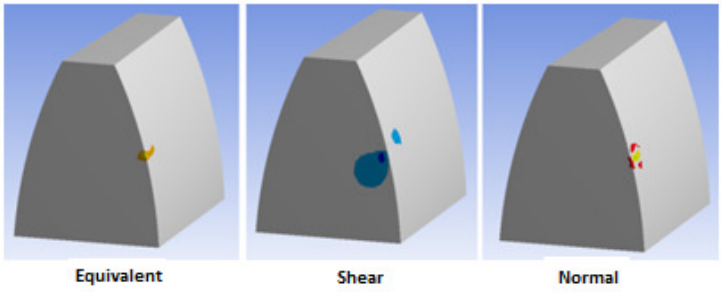

Figure 8. Stresses in convex-convex contact using MPC method.

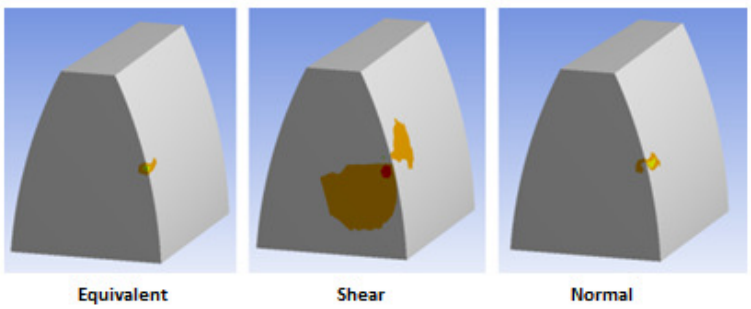

Figure 9. Stresses in convex-convex contact using Normal Lagrange method.

In convex-concave configuration there is a similarity in shape and amplitude of equivalent stress gradients in all methods. In Figures 10-12 results of methods used were illustrated. In normal stress results, similarity occurs between MPC and Pure Penalty methods. However, in shear results, stressed regions are different with asymmetric amplitudes. Differences in results are obtained from characteristics of each contact mechanism and because of differences in contact areas as seen in gradients of each method used. In this case, it was verified that in all methods there are two points of contact on tooth face and this behavior was not expected, even with an interactive method changing the contact parameters, the gradient persisted. This can justify the high error compared to the analytical method, since only one elliptical-shaped contact point was foreseen.

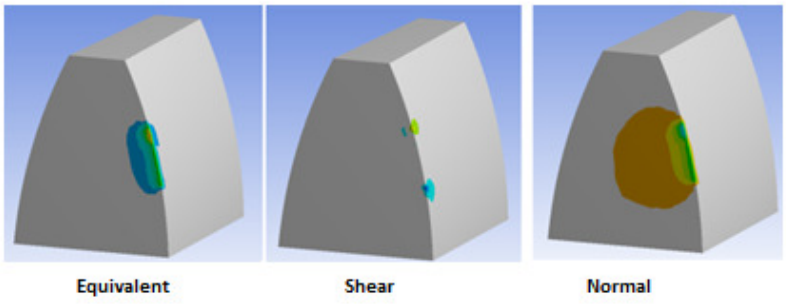

Figure 10. Stresses in the convex-concave contact using the Pure Penalty method.

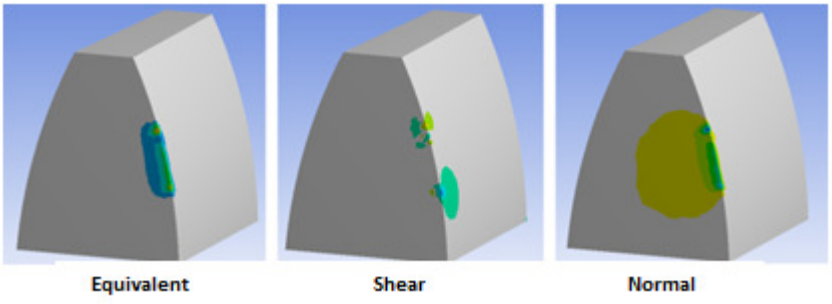

Figure 11. Stresses in the convex-concave contact using the MPC method.

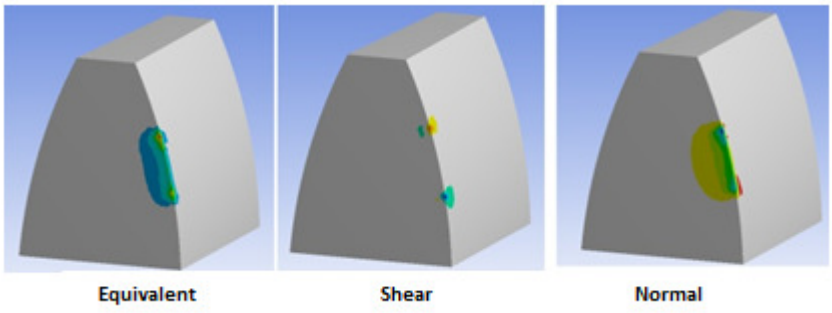

Figure 12. Stresses in the convex-concave contact using Normal Lagrange.

5. CONCLUSION

Analyzing the results of normal contact stresses from analytical and numerical studies, the Pure Penalty method in convex-convex configuration obtained closest result to analytical method while the Normal Lagrange method obtained the smallest difference in convex-concave case.

It was verified that the shear stress has a lot of influence on the result as shown in Figure 6, mainly in the equivalent stress where it has a similar curve behavior due to its great influence on the material distortion. Considering the shear stress, the Pure Penalty method obtained the closest results to the analytical method in both configurations.

Considering the behavior of the results obtained in the numerical method, it is observed that the areas where the generated stresses act are different even though the characteristics of meshes and constraints used are identical between the three methods. In Figures 7-9 the results of the convex-convex contact methods show a significant difference in the amplitude of the normal and shear stress gradients, while the regions bounded by equivalent stresses are similar in the MPC and Lagrange methods. In the convex-concave configuration, there is a similarity in shape and amplitude of the equivalent stresses gradients in all methods as shown in Figures 10-12. In the case of normal tension, there is a similarity between the MPC and Pure Penalty methods. Even with the similarity of the stresses amplitude format (in relation to the other two methods), the percentage difference obtained in the MPC results in relation to the analytical method exceeded 99%. The interactions with the pinball region had no effect for the result to converge with the expected. Therefore, in this case, the MPC method with the configurations used was not viable for the convex-concave study.

The cause of the variation in the results can be generated by the area recognized in the contact between the solids, as shown in Chart 2, the contact detection in the Normal Lagrange and MPC methods takes place at the nodes while in the Pure Penalty method it takes place at the integration points. In this specific case with curved surfaces the contact without separation can influence the contact region in an erroneous way with the use of the pinball region. If the radius value of this region is beyond what is necessary the software can generate closed contact in distant areas enlarging the interaction region also affecting the number of nodes included in the equations of all methods. Thus, it can lead to a sampling space where the mathematical model used is restricted and ineffective.

In the numerical study of the hypothetical gear (convex-concave) it was found that in all methods there are two contact points on the tooth face and this behavior was not expected even with an interactive method changing the contact parameters the gradient persisted. This can be caused by the hypothetical gear face not being suitable for the envolvental curve with the parameters used in the gear.

6. ACKNOWLEDGEMENTS

The authors would like to thank the *"Coordenação de Aperfeiçoamento de Pessoal de Nível Superior - Brasil (CAPES)"*.

7. REFERENCES

Ali, F. 2020. Numerical Study on Subsurface Stress in Hertzian Contacts under Pure Sliding Conditions. Journal of Applied and Computational Mechanics, 6(Special Issue), 1098-1106.

Andrei, L., Epureanu, A., Andrei, G., Birsan, I., & Walton, D. 2005. Synthesis and analysis of plastic curved-face-width spur gears. VDI BERICHTE, 1904(2), 1781.

ANSYS. 2007a. Contact technology guide. Ansys Release 11.0.

ANSYS. 2015b. ANSYS Mechanical User's Guide.

Azarov, A. D.; Zhuravlev, G. A. 2017. Influence of cylinder curvature on the maximum shear stress at contact. Russian Engineering Research, v. 37, n. 1, p. 13-18.

Bergseth. E., & Björklund, S. 2010. Logarithmical crowning for spur gears. Journal of Mechanical Engineering v.56(4), p. 239-244.

Brezeanu, Ligia Cristina. 2015. Contact stresses between two cylindrical bodies: cylinder and cylindrical cavity with parallel axes–Part I: Theory and FEA 3D modelling. Procedia Technology, v. 19, p. 169-176.

Chandra, D. et al. 2016. Fatigue growth analysis of a surface crack in a solid cylinder under combined cyclic axial-torsion loading. Experimental Techniques, v. 40, n. 5, p. 1397-1407.

Guidi, Erick Siqueira; De Azevedo Silva, Fernando, 2013. Analysis of Fatigue Failure in the Rolling Bearings. SAE Technical Paper.

Halling, J. 1975. Principles of tribology, McMillan, London pp. 56-60.

Hattori, G., & Serpa, A. L. 2015. Contact stiffness estimation in ANSYS using simplified models and artificial neural networks. Finite Elements in Analysis and Design, 97, 43–53.

Hwang, Seok-Chul et al. 2013. Contact stress analysis for a pair of mating gears. Mathematical and Computer Modelling, v.57, n. 1-2, p. 40-49.

Juvinall R.C., Marshek K.M. 2008. Projeto de Componentes de Máquinas. Grupo Gen-LTC

Kalker, J. J. 1990. Three-Dimensional Elastic Bodies in Rolling Contact (Vol. 2). Springer Science & Business Media.

KHK, 2021. Available in https://khkgears.net/new/gear_knowledge/gear_technical_reference/ involute_gear_ profile. html. Accessed in feb. 2021.

Köhn, André Oliveira; De Azevedo Silva, Fernando, 2020a. A numerical and analytical study of the stress field generated by the contact between a rail and a wheel. SN Applied Sciences, v. 2, n. 7, p. 1-8.

Köhn, André Oliveira; Silva, Fernando Azevedo, 2020b. Un estudio del campo de tensión generado por el contacto entre una esfera y una placa plana para un modelo simplificado de rodamientos rígidos de bolas. Ingeniería e Investigación, v. 40, n. 2.

Lanoue, F., Vadean, A., & Sanschagrin, B. 2009. Finite element analysis and contact modelling considerations of interference fits for fretting fatigue strength calculations. Simulation Modelling Practice and Theory, 17(10), 1587-1602. doi:10.1016/j.simpat.2009.06.017.

Masao Kubota, Haguruma Nyumon, 1963. Tokyo, Ohmsha, Ltd.

Norton R.L. 2013. Projeto de máquinas. Bookman, Brazil.

Purushothaman, Prabhakar & Thankachan, Prashanth. 2014. Hertz Contact Stress Analysis and Validation Using Finite Element Analysis. International Journal for Research in Applied Science and Engineering Technology (IJRASET). 2. 521-538.

Rycerz, Pawel; Olver, Andrew; Kadiric, Amir. 2017. Propagation of surface initiated rolling contact fatigue cracks in bearing steel. International Journal of Fatigue, v. 97, p. 29-38.

Sackfield, A., & Hills, D. A., 1983. Some useful results in the classical Hertz contact problem. The Journal of Strain Analysis for Engineering Design, 18(2), 101–105.

Stefancu, Andrei-Ionut; Melenciuc, Silviu-Cristian; Budescu, Mihai. 2011. Penalty based algorithms for frictional contact problems Buletinul Institutului Politehnic din lasi. Sectia Constructii, Arhitectura, v. 57, n. 3, p. 119.

Tallian, T. E. 1967. On competing failure modes in rolling contact. ASLE transactions, v. 10, n. 4, p. 418-439.

Timoshenko, S. P. and Goodier, J. N. 1970. Theory of elasticity. 3rd edition, McGraw-Hill, New York pp.414-420.

XIE, Yuan-pi; FENG, Gang. 2009. Study of ANSYS modelling on the combination of 3D entity unit and plate-shell unit [J]. Journal of Machine Design, v. 4.

Zhang, B. Q., He, J. X., & Qiao, Y. F. 2012. The Application of ANSYS Multipoint Constraint on the Combination Modeling of SOLID-SHELL. Advanced Materials Research, 588-589, 226–229.

8. **RESPONSIBILITY NOTICE**

The authors are the only responsible for the printed material included in this paper.